Deployable Antennas for CUBE Satellites in Low Earth Orbit

For detection of ADS-B signals

Master thesis

Karsten Schou Nielsen

Aalborg University
Department of Electronic Systems
Fredrik Bajers Vej 7B
DK-9220 Aalborg

Here you can write something about which tools and software you have used for typesetting the document, running simulations and creating figures. If you do not know what to write, either leave this page blank or have a look at the colophon in some of your books.

Department of Electronic Systems
Fredrik Bajers Vej 7
DK-9220 Aalborg Ø
http://es.aau.dk

AALBORG UNIVERSITY
STUDENT REPORT

Title:
Deployable Quadrifilar Helical Antenna for space application

Theme:
Scientific Theme

Project Period:
Fall Semester 2018

Project Group:
XXX

Participant(s):
Karsten Schou Nielsen

Supervisor(s):
Ming Shen

Copies: 1

Page Numbers: 33

Date of Completion:
March 26, 2019

Abstract:

Here is the abstract

Institut for Elektroniske Systemer
Fredrik Bajers Vej 7
DK-9220 Aalborg Ø
http://es.aau.dk

AALBORG UNIVERSITET
STUDENTERRAPPORT

Titel:
Deployable Quadrifilar Helical Antenna for space application

Tema:
Semestertema

Projektperiode:
Efterårssemestret 2018

Projektgruppe:
XXX

Deltager(e):
Karsten Schou Nielsen

Vejleder(e):
Ming Shen

Oplagstal: 1

Sidetal: 33

Afleveringsdato:
26. marts 2019

Abstract:

Her er resuméet

Contents

Todo list

Preface

Here is the preface. You should put your signatures at the end of the preface.

Aalborg University, March 26, 2019

Author 1
<username1@XX.aau.dk>

Author 2
<username2@XX.aau.dk>

Author 3
<username3@XX.aau.dk>

Chapter 1

Introduction

The goal of this project is to make an deployable antenna for Automatic dependent surveillance-broadcast (ADS-B) on a Low-Earth Orbit (LEO) satellite. ADS-B is a system in which aircraft continually transmit their identity and GPS-derived navigational information. ADS-B networks for air traffic monitoring have already been implemented in areas around the world, but ground stations cannot be installed in mid-ocean and are difficult to maintain in the Arctic, leaving a coverage gap for oceanic and high latitude airspace. Therefore a solution can be to monitor the signals with a low orbit satellite using an antenna matched to the frequencies of the ADS-B. This has already been done by the company Aireon which has 66 ADS-B receivers hosted on the new Iridium NEXT LEO satellite constellation. But this is a large satellite and a CubeSat would be better suited for the application. Therefore the antenna should fit in a 1U cubesat which can be deployed when in space.

Chapter 2

Linkbudget

2.1 ADS-B signals

There are currently three types of ADS-B transmissions but for satellite reception only the 1090 MHz extended squitter (ES) is of interest. An ADS-B message is 112 bits long and the transmission takes 120us. The modulation is Binary Pulse Position Modulation (BPPM) and the package consist of 5 parts. The first part is Downlink Format which tells that this is an ADS-B signal, second part is Additional Identifier which has different meaning within each ADS-B subtype. The third is the ICAO which is the unique identifier of the aircraft. The fourth is the DATA which contains several informations including aircraft operation status, airborne position and velocities measured from different sensors. The fifth and last is the checksum [Sun, 2015].

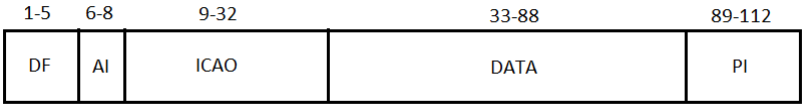

Figure 2.1: 112 bit long ADS-B message

2.2 Free space loss

Typically in satellite communication a LOS component exist. Therefore the only obstacle between the satellite and user is the atmosphere and therefore the loss can be modelled as free space, with a limited variation due to weather conditions. ADS-B signal is sent through a linear polarized monopol with power varying from 125W to 500W depending of the airplane and speed [Francis, 2011]. The height of a Low Earth Orbit (LEO) satellite is between 600 km to 800 km. To calculate the power loss Friis Transmission Equation is used.

$$\frac{P_r}{P_t} = (\frac{\lambda}{4\pi R})^2 G_t G_r |\vec{Pr} \cdot \vec{Pt}|^2 \tag{2.1}$$

$$\lambda = \frac{c}{f} \tag{2.2}$$

Where $c = 3e8$ is speed of light in vaccum and f is the frequency in Hz. $|\vec{Pr} \cdot \vec{Pt}|^2$ denotes polarization mishmash.

2.3 LEO coverage

For a satellite the coverage area on the earth is a circular area which is defined by the height (H) of the satellite and the angel α_0. The maximum distance the signal travels from the satellite to the earth and vice versa, is d which is depicted in figure 2.2 [Shkelzen Cakaj, 2014]. The equation for d is given by equation 2.3

$$d = R_e(\sqrt{(\frac{H + R_e}{R_e})^2 - \cos^2 \epsilon_0} - \sin \epsilon_0) \tag{2.3}$$

Where

$$\epsilon_0 = \arccos \frac{\sin \alpha_0 (R_e + H)}{R_e} \tag{2.4}$$

and $R_e = 6378km$ is the radius of the earth. Further the coverage percentage of the satellite can be calculated by equation 2.5 which uses the total area of the earth divided by the area covered by the satellite.

$$Coverage(\%) = \frac{A_{coverage}}{A_{earth}} = \frac{2\pi R_e^2 (1 - \cos \beta_0)}{4\pi R_e^2} \cdot 100\% \tag{2.5}$$

$$\beta_0 = 90 - \alpha_0 - \epsilon_0 \tag{2.6}$$

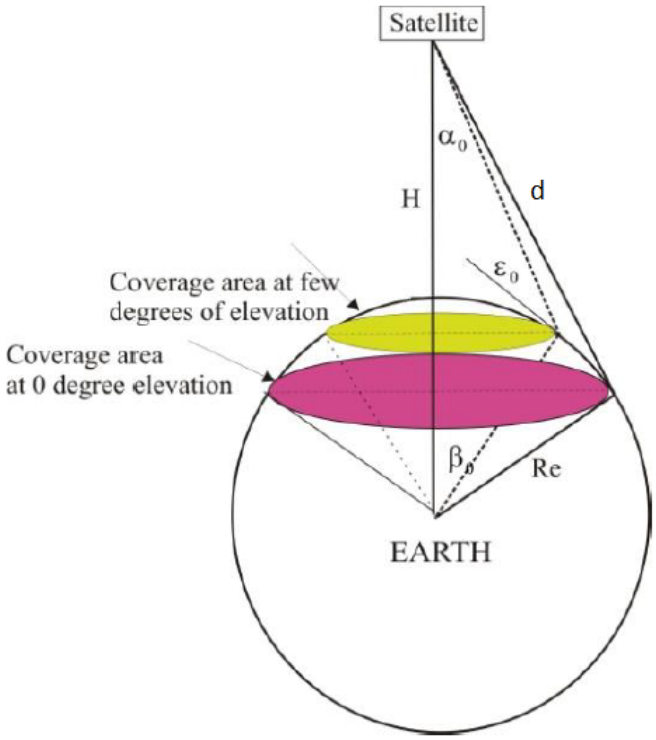

Figure 2.2: Earth coverage for a satellite. Pink area is maximun coverage, green is area limited to the antenna beamwidth. [Shkelzen Cakaj, 2014]

Because of the geometry of the earth and the height of the satellite a maximum coverage area must exist. This is depicted in figure 2.2 as purple area. To find the maximum angle of α_0 equation 2.7 is used.

$$\alpha_0(max) = \arcsin \frac{R_e}{R_e + H} \tag{2.7}$$

2.4 LEO radiation pattern

Because of the unknown factor of which direction the signal arrives and which polarization the signal has, a circular polarized antenna is best suited for satellite communication [Balanis, 2005]. Depending on the application it can ether be the ground station or satellite which polarization is circular. In this project it is desired to have the circular antenna placed at the satellite because ADS-B signals is transmitted by a linear monopole [ITU-R, 2017] attached to the top or bottom of the aircraft, depending of the size of the aircraft. As described earlier the signal does not always travel the same distance and therefore the loss is diffrent due to the angle of reception. The farfield of the satellite antenna should therefore compensate for this by letting the gain increase due to the angle, which is depicted in figure 2.3.

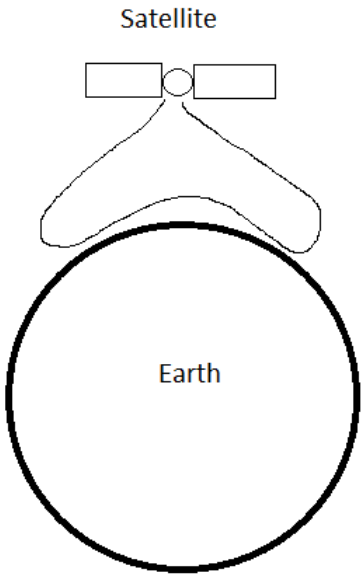

Figure 2.3: Desired farfield for a LEO satellite

Knowing equation (2.3) and (2.4) a plot of the farfield can be calculated. This is done by equation (2.8) where $d()$ is equation (2.3). The formula normalizes the gain to an angle of zero. A plot showing the relative gain at diffrent heights is shown in figure 2.4. It is also seen from equation 2.8 that the loss due to the angle is frequency independent.

$$G_r(\alpha) = 10 \cdot log_{10}(\frac{(\frac{\lambda}{4\pi d(0)})^2}{(\frac{\lambda}{4\pi d(\alpha)})^2}) = 10 \cdot log_{10}(\frac{d(\alpha)^2}{d(0)^2}) \tag{2.8}$$

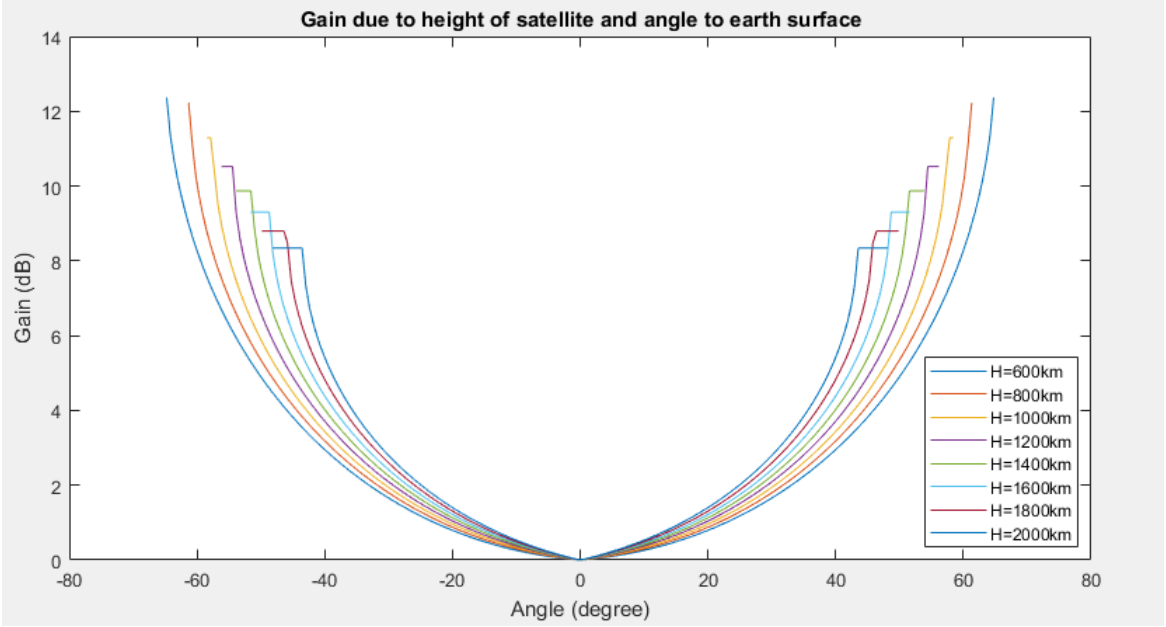

Figure 2.4: Normalized gain requirement for a LEO satellite at different heights

Table 2.1: scaling factor

Height	*Max coverage*	*Max angle*
600km	3.9%	64.7°
800km	4.9%	61.4°
1000km	5.8%	58.6°
1200km	6.7%	56.2°
1400km	7.4%	54.0°
1600km	8.1%	52.0°
1800km	8.6%	50.2°
2000km	9.1%	48.6°

2.5 Tabel

With the previously description is it now easy to calculate a linkbudget. It is assumed that the receiving antenna is a circular polarized antenna which will cause a polarization mismatch at -3dB [Balanis, 2005]. Futher an atmospheric loss at 0.1dB is assumed together with a carier to noise radio at minimum 9dB [ITU-R, 2017]. Loss due to cables or connectors has not been taken into account. The system noise temperature is set to 373K because of the high temperature span in the LEO [Francis, 2011]. The calculations is done at a transmit power at 125W and 500W which is the minimum and maximum transmit power due to the standard.

Table 2.2: Linkbudget for 1090MHZ and H = 800km

Item	*Link parameter*	*Value*	*Unit*	*Computation*
1	Frequency	1090	MHz	
2	Transmit power (125W)	21.0	dB	
2	Transmit power (500W)	27.0	dB	
3	Transmit antenna gain	3.0	dBi	
4	Athmospheric absorbtion (clean air)	0.1	dB	
5	Free-space loss	151.2	dB	
6	Polarisation loss	3.0	dB	
7	Received carrier power	-130.3	dB	2+3-4-5-6
8	Bandwith (4.6MHz)	66.6	dB Hz	
9	System noise temperature (373K)	25.7	dBK	
10	Boltzmann's constant	-228.6	dBW/Hz/K	
11	Noise power	-136.3	dBW	8+9+10
12	Carrier to noise ratio	6.0	db	7-11
13	C/(N+I)	9.0	db	Requirement
14	Antenna gain at 125W and $\alpha_0 = 0$	3.0	db	13-12
15	Antenna gain at 125W and $\alpha_0 = \alpha_{max}$	15.0	db	14+equation 2.7
16	Antenna gain at 500W and $\alpha_0 = 0$	-3.0	db	13-12
17	Antenna gain at 500W and $\alpha_0 = \alpha_{max}$	9.0	db	14+equation 2.7

Chapter 3

Antennas

In this section different antenna types is analysed and simulated in CST studio. Simple structures such as monopoles and dipoles is not considered since the polarization in the antennas basic form is linear. Even though it is possible to make a crossed dipole array that is circular polarized and have a high gain, but this structure would become large and still not have the opportunity to form the radiation pattern as required. Other structures such as spiral antennas and conical antennas is neither considered since those primarily is used as wideband antennas. This section will investigate the possibility to form the radiation pattern to a field to overcome the requirements from chapter 2 only.

3.1 Reflector Antennas

Reflector antennas are used places where a high gain is needed. The reflector antenna do also have a wide bandwith, which all together has made them popular for deep space communication [William A. Imbriale, 2012]. Although reflector antennas can be made in different types, shapes and configurations, they all essentially consist of a passive reflecting surface illuminated by a smaller primary feed. The basic analysis is done using trigonometry which provides satisfactory result because the diameter of the reflecting surface often is ten times the wavelength. In figure 3.1 four main configurations is depicted. (a) is the on-focus parabolic reflector where the feed for the parabolic is placed F distance apart called the focal point. This would leave an area where the feed is placed, where there will be a gap in the coverage. This is omitted in (b) which is the off-axis reflector. This types has no gap in coverage and therefore is often used as radar. The (c) Cassegrain reflector and (d) Gregorian reflector uses both a feed in the middle of the reflector which then uses a second reflector at the focal point to reflect the energy back to the large reflector. Because of the large dimensions a reflector antenna are not suited for low frequencies $<$ 2GHz. Using the equations 3.1 to 3.1 a design has been made for $f = 10GHz$, $\lambda = 30mm$, $D = 10\lambda = 300mm$, $\theta = 60°$. This should give a gain at 30dBi. The design has been simulated in CST studio in figure 3.2 and 3.3. The feeding antenna used is a

dipole which is an omnidirectional antenna, this causes a loss in efficiency. An ideal reflector should be uniformly illuminated and all power should be focused on the reflecting surface. The portion of the feed power that does not reach the reflector is referred to as spillover loss while the ability to uniformly feed the parabola is referred to as illumination efficiency. Since primary feeds have a tapered radiation pattern, a compromise between spillover losses and illumination efficiency must be considered to maximize the aperture gain. In the simulation a gain at $G = 15dB$ was obtained, this could be optimized using an horn-antenna.

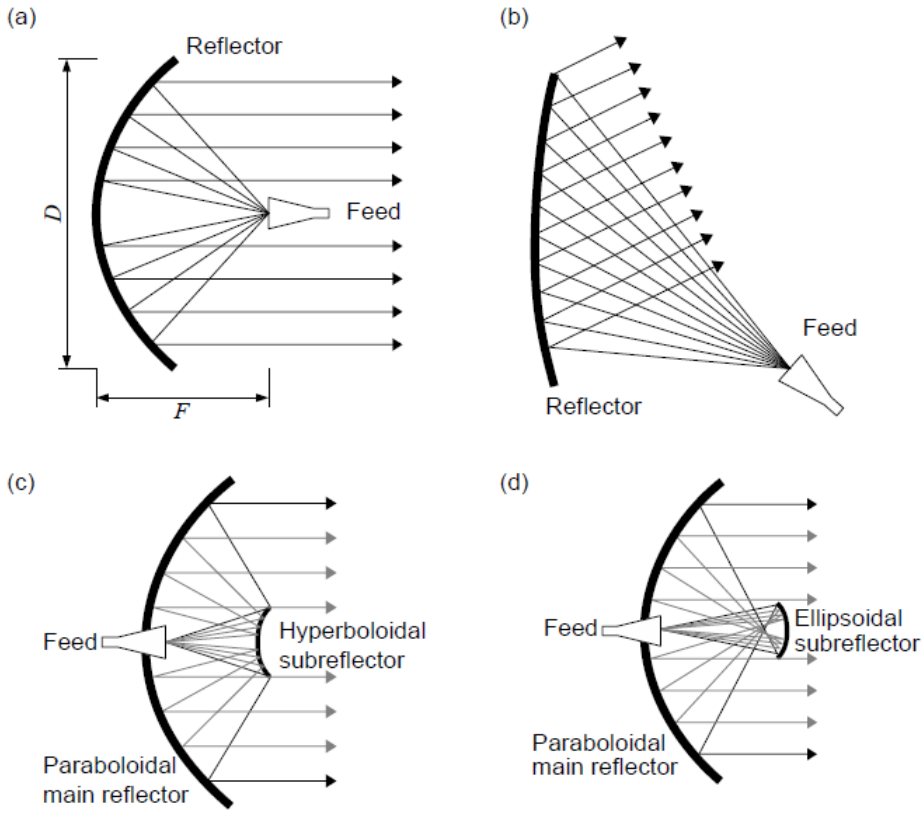

Figure 3.1: Reflector antenna configurations: (a) on-focus parabolic reflector; (b) off-axis reflector; (c) Cassegrain reflector; (d) Gregorian reflector [William A. Imbriale, 2012]

Equation for parabola

$$y = ax^2, a = \frac{1}{4F} \tag{3.1}$$

Focal length

$$F = D\frac{1}{4tan(\theta/4)} \tag{3.2}$$

Length of parabolic segment

$$L = \frac{ln(\sqrt{a^2D^2+1}+aD)}{4a} + \frac{D\sqrt{a^2D^2+1}}{4} \tag{3.3}$$

Gain for parabolic reflector

$$G = \eta\frac{4\pi A}{\lambda^2}, A = \frac{\pi D^2}{4} \tag{3.4}$$

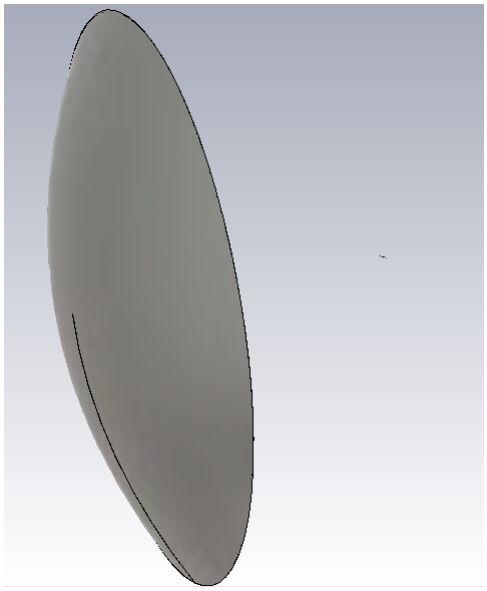

Figure 3.2: Simulated reflector antenna in CST studio

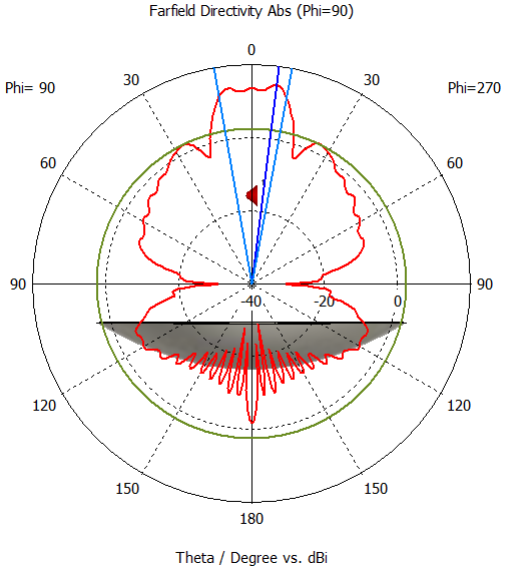

Figure 3.3: Farfield of simulated reflector antenna in CST studio

3.2 Helical Antennas

3.2.1 Helical antenna with ground plane

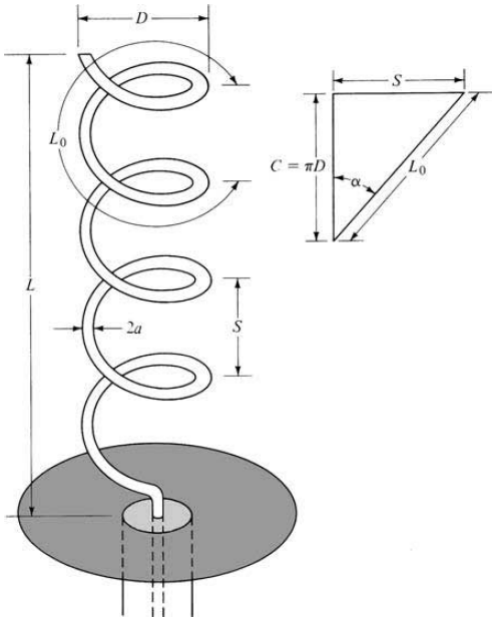

Figure 3.4: Helical antenna with ground plane [Balanis, 2005]

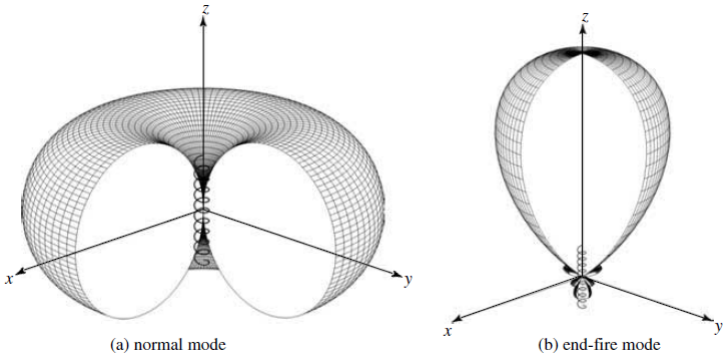

Figure 3.5: Farfield for (a) normal mode and (b)end-fire mode in linear scale [Balanis, 2005]

A helical antenna is a wire wound in form of a screw and is depicted in figure 3.4. The helical antenna consist of N turns, diameter D and spacing between the turns S and circumference is $C = \pi D$ where the total length is $L = NS$. Normally the helical antenna has a circular ground plane with the diameter $G_d = \frac{3\lambda}{4}$. Another important parameter is the pitch angle α which is the angle formed by a line tangent to the helix wire and a plane perpendicular to the helix axis. The pitch angle is defined by

$$\alpha = tan^{-1}(\frac{S}{\pi D}) = tan^{-1}(\frac{S}{C}) \tag{3.5}$$

The radiation pattern of the antenna can be varied by controlling the size of its geometrical properties compared to the wavelength. The input impedance is critically dependent upon the pitch angle and the size of the conducting wire, especially near the feed point, and it can be adjusted by controlling their values. The general polarization of the antenna is elliptical. However circular and linear polarizations can be achieved over different frequency ranges [Balanis, 2005]. The helical antenna can operate typically in one of two modes which is the normal (broadside) and the axial (end-fire) mode see figure 3.5. In end-fire mode a circular polarization is archived if the D and S is large fractions of the wavelength. The design criteria is $\frac{3}{4} < C/\lambda < \frac{4}{3}$ where $C = \lambda$ is optimum. $S = \frac{\lambda}{4}$ this gives a pitch angle between $12^o \leq \alpha \leq 14^o$ and a ground plane at least $G_d = \frac{\lambda}{2}$. Formulas for radiation resistance Half Power Beam Width (HPBW) and reflection coefficient is given by equation 3.2.1 to 3.2.1. The formulas has an accuracy about 20% the formulas are therefore held up with a simulation at $f = 1GHz$.

Directivity

$$D = 15N\frac{C^2 S}{\lambda^3} = 12.7dB \tag{3.6}$$

Half Power Beam Width

$$HPBW = \frac{52\lambda^{3/2}}{C\sqrt{NS}} = 46.5^o \tag{3.7}$$

Impedance of antenna

$$Z_l = 140\frac{C}{\lambda} = 140\Omega \tag{3.8}$$

Reflection coefficient

$$\Gamma = \frac{Z_l + Z_s}{Z_l - Z_s} = -3.2dB \tag{3.9}$$

The simulation results are depicted in figure 3.6 to 3.8. It can be seen that the simulated results corresponds well with the formulas whit in 20% accuracy. Even though the shape of the radiation pattern can be adjusted by varying the shape of the helix, it it not possible to obtain circular polarization in those "custom" shapes and therefore the helix cannot be used for tracking of ADS-B signals other than in the end-fire mode.

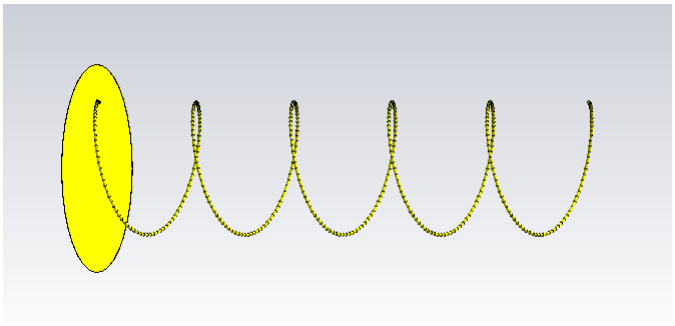

Figure 3.6: Simulated helical antenna

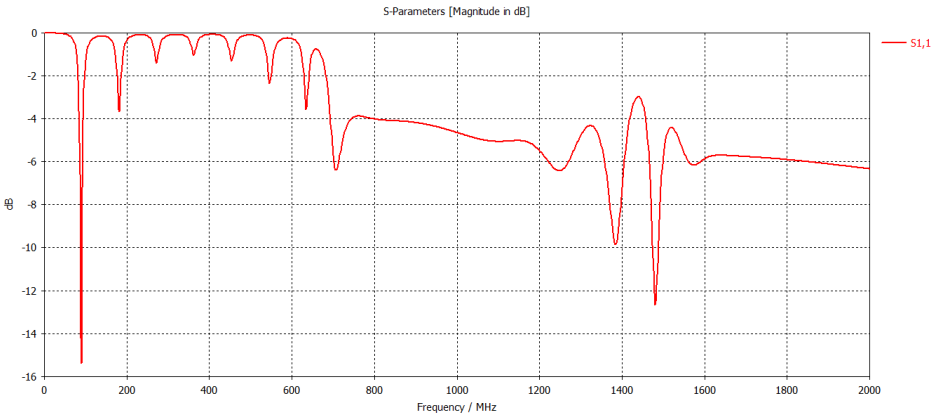

Figure 3.7: Reflection coefficient for simulated helical antenna

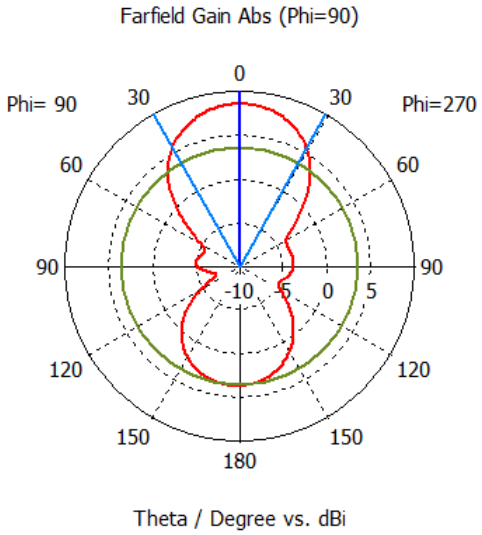

Figure 3.8: Farfield for simulated helical antenna with a maximum gain at 8.5dB and a HPBW at 58.8^o. This gives a coverage percentage at the earth at 0.5%

3.2.2 Quadrifilar Helical Antenna

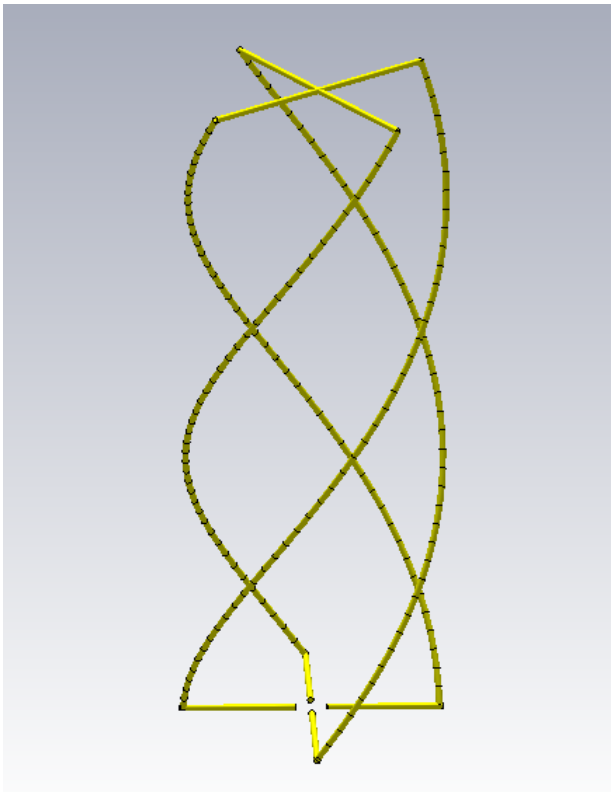

Figure 3.9: QHA with $N = 0.6$, $D = 80mm$,$L = \frac{\lambda}{2} - D \cdot 0.75$, $f = 1GHz$

The Quadrifilar Helical Antenna (QHA) (see figure 3.9) is an resonant antenna which is typically feed by two ports with a 90° phase difference. The antenna has a circular polarization and the size is often smaller than a normal helical antenna. Typically the length of each arm is an integral multiple of the quarter-wavelength. The end of the helix is open when the integer is odd, while short when the integer is even [Xudong Bai, 2014]. Despite the typically design the turn ratio, radius, length and feeding topology will affect the radiation pattern and polarization.

An QHA has been build and simulated in CST studio. The dimensions are $D = 80mm$,$L = \frac{\lambda}{2} - D \cdot 2$, $N = 0.6$ at the frequency $f = 122.5MHz$ and $\lambda = 2450mm$ with the wire diameter $Wd = 2mm$. The length is calculated so there is a half wavelength for the current flow between the negative and positive side of a port. The feeding is done using two discrete ports as shoved in figure 3.10.

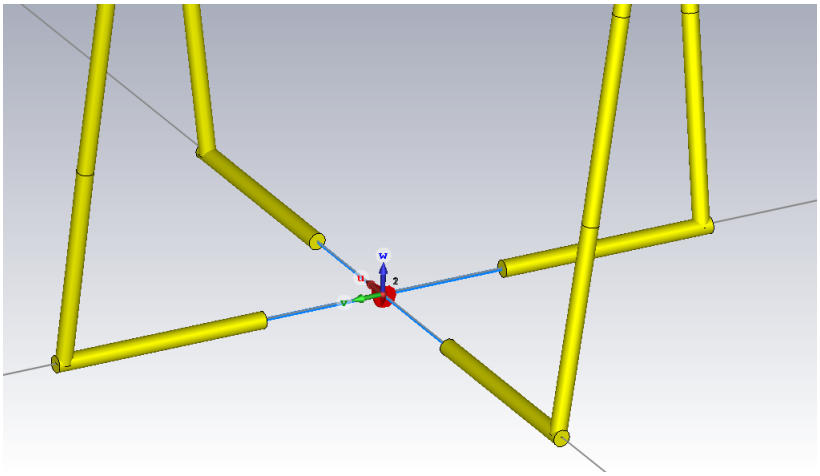

Figure 3.10: Feeding of the QHA for 122.5MHz using discrete ports

The QHA has been simulated and the results shows, that the antenna is resonating at 131MHz even thou the S11 parameter at this frequency is only -2dB, see figure 3.11. The small difference in frequency due to the calculations is caused by the gap between the ports in the bottom and the extra length caused by the turn of N. It can be seen that the antenna also radiates at multiply of the first resonant frequency and that the lowest return-loss is obtained at 4 times the frequency which gives 519MHz. The farfields for the frequencies 131,262,393 and 519MHz are shown in figure 3.12, 3.13, 3.14 and 3.15, where port 1 is fed with a positive phase at 90°. It is seen that the farfield not surprisingly changes with the frequency and that a higher frequency will result in side lobes. This could be an advantage to overcome the requirement from figure 2.3 but unfortunately the polarization becomes linear in the angle of the sidelobes which then makes this option unuseful.

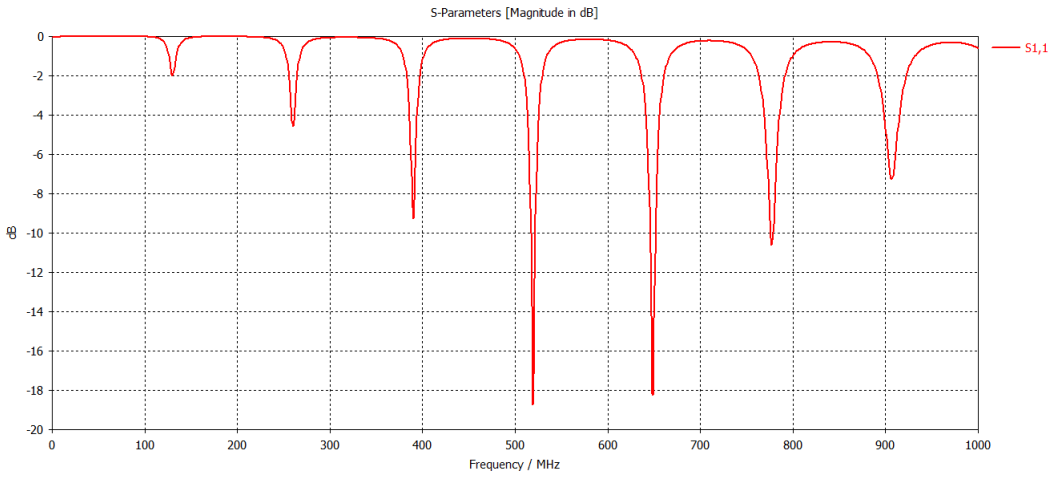

Figure 3.11: S11 parameter of the QHA for 122.5MHz

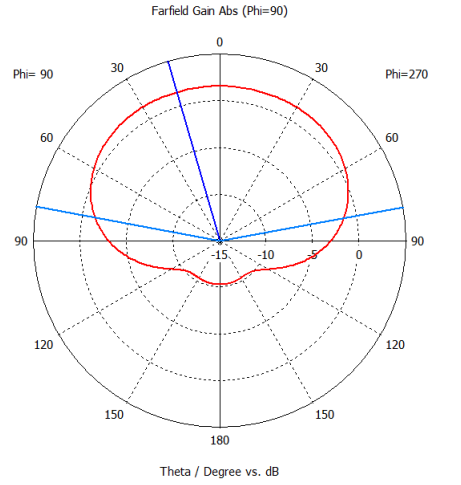

Figure 3.12: Simulated farfield at 131MHz

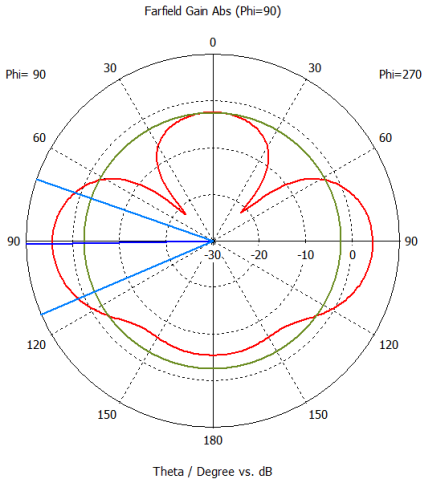

Figure 3.13: Simulated farfield at 262MHz

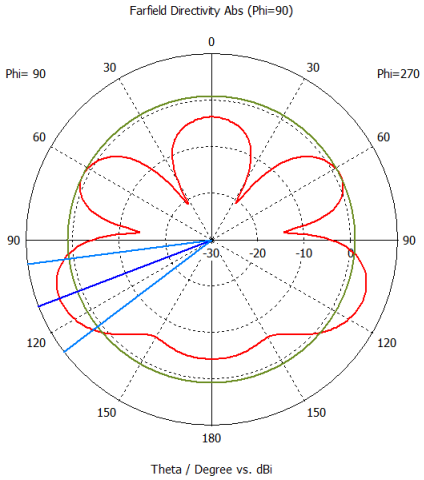

Figure 3.14: Simulated farfield at 393MHz

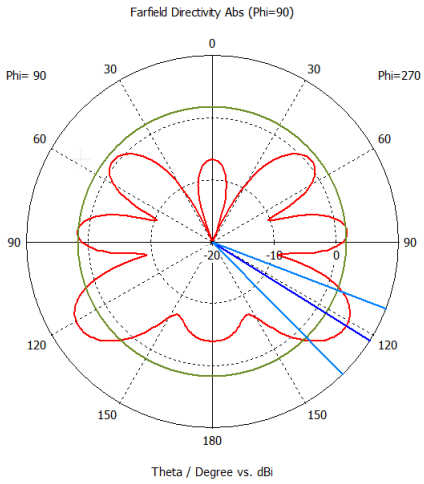

Figure 3.15: Simulated farfield at 519MHz

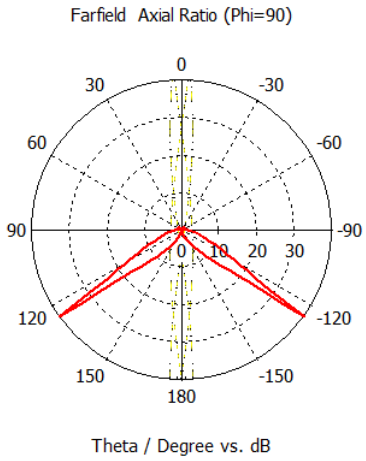

Figure 3.16: Simulated Axial Ratio at 131MHz

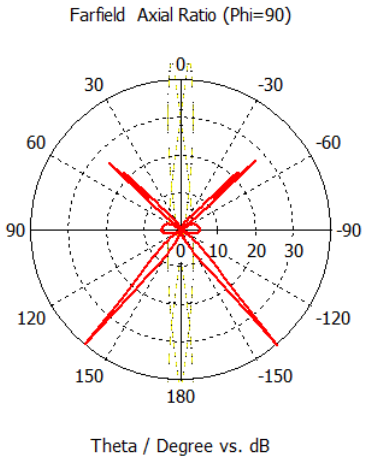

Figure 3.17: Simulated Axial Ratio at 262MHz

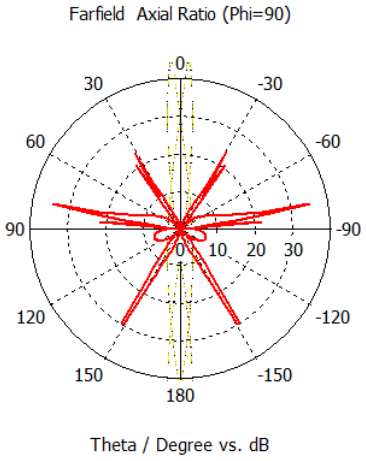

Figure 3.18: Simulated Axial Ratio at 393MHz

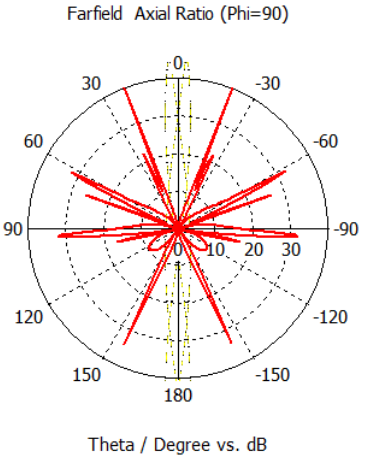

Figure 3.19: Simulated Axial Ratio at 519MHz

Feeding methods

In figure 3.10 the feeding of the QHA is done using two discrete ports. When port 1 is fed with a positive phase at 90° the QHA will have it's maximum radiation in the forward direction. If the port instead is fed with a negative phase at 90° then the QHA will have it's maximum radiation in the backward direction. Other phases will result in non-uniform radiation patterns with one ore more peaks in the azimuth axis. It is easy to believe that it is possible to connect two of the arms of the QHA to a common ground and feed the one port with a phase difference at 90° using a $1/4\lambda$ transmission-line and the other directly from the source depicted in figure 3.20. But this will not work since the geometry of the QHA will change

from an electrically perspective. The shortening of the two grounds will affect the flow of the current resulting of only a pattern difference of 45° in the farfield which then makes it impossible to archive a omnidirectional radiation pattern and circular polarization. To overcome this is has been shown in [Xudong Bai, 2014] that it is possible to use a feeding network consisting of one second-iteration Moore 180° hybrid coupler and two second-iteration Sierpinski 90° hybrid couplers. It has also been showen in [Xiaoqiang Yang, 2014] that a broadband feed network can be done using an wilkinson powerdivider and broadband 90° phase shifters.

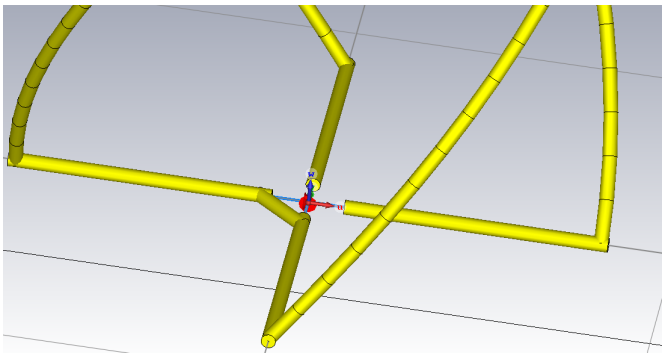

Figure 3.20: Common GND for the QHA

Wideband QHA

As shown previously a QHA in its basic form radiates only at a narrow frequency band. For the S-parameters in figure 3.11 it is seen that at 131MHz the return loss is about -2dB which results in an efficiency at only -5dB. This can be improved using a match network, but the antenna still needs to be a radiating element and therefore the matching can only improve the return-loss and not the bandwidth [Iyer, 2010]. Therefore some modifications needs to be done at the QHA to improve the bandwidth. One method is to make the bifilar arms of the QHA in diffrent lengths so one arm is longer than the resonant frequency and the other shorter as depicted in figure 3.21. The feeding is done by shortening the feeds as in figure 3.22 and feed with a $1/4\lambda$ coax cable as balun. Because the feeding is done this way the farfield will not be omnidirectional and is skewed in one direction as depicted in figure 3.23 but still useful in some applications. The S-parameter in figure 3.24 shows a bandwidth at 10% which is limited by the $1/4\lambda$ balun. This could be improved, but the farfield will then change and the improvements will be doubtful.

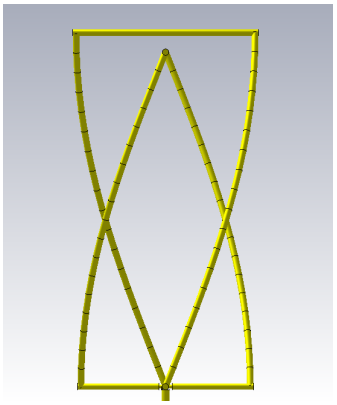

Figure 3.21: Wideband QHA with dimentions $f = 1GHz$, $\lambda = 300mm$, $R1 = \lambda 0.091$, $L = \lambda 0.36$, $R2 = \lambda 0.086$, $L = \lambda 0.34$

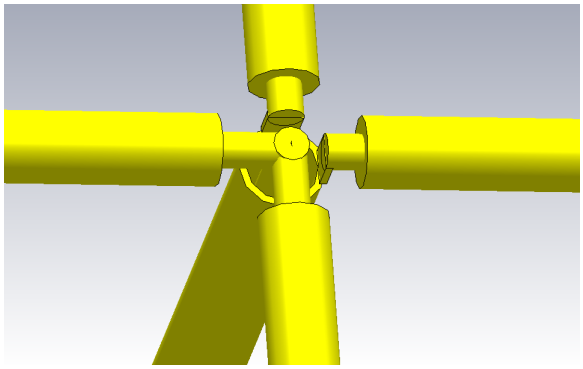

Figure 3.22: Feeding for the wideband QHA

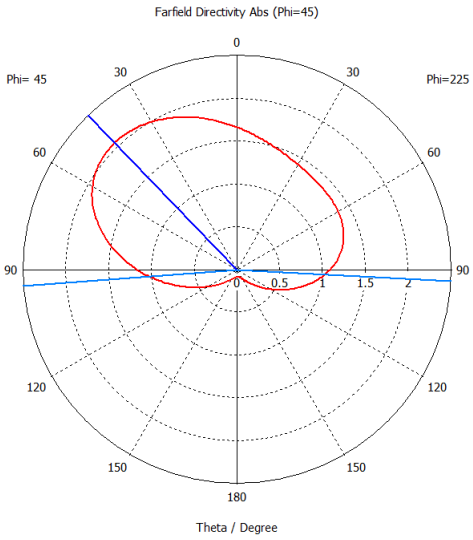

Figure 3.23: Farfield for the wide band QHA in linear scale

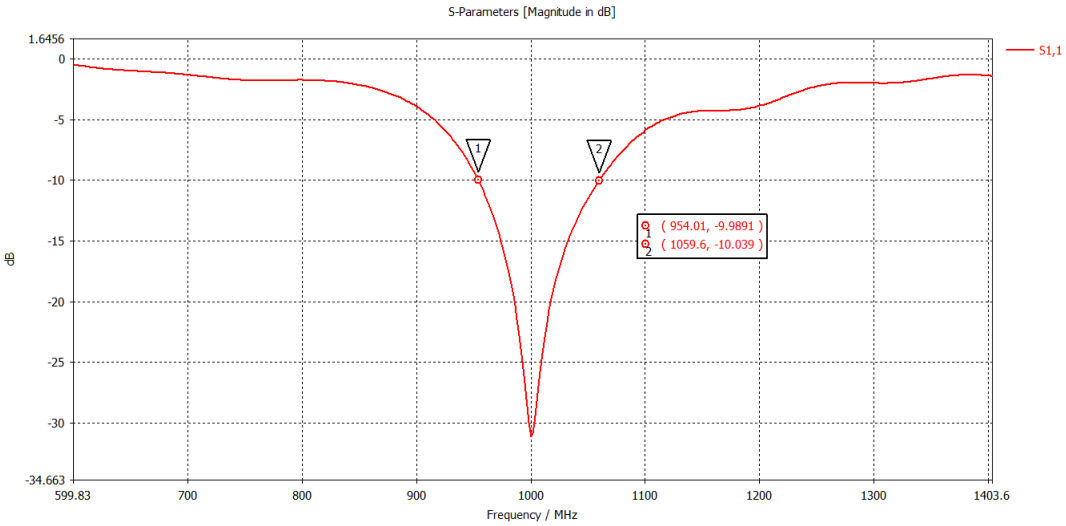

Figure 3.24: S-parameters for the wideband QHA shows a bandwidth at 10%

Multiband QHA

Another configuration of the QHA is the Multiband QHA [Xudong Bai, 2014] which can be build up on several narrowband or wideband QHA's inside each other as depicted in figure 3.25. This configuration allows several frequency bands to be covered since several QHA's can be build inside each other. The consequence is though a heavy and complex design which may also needs a complicated feeding network or several ports for each frequency.

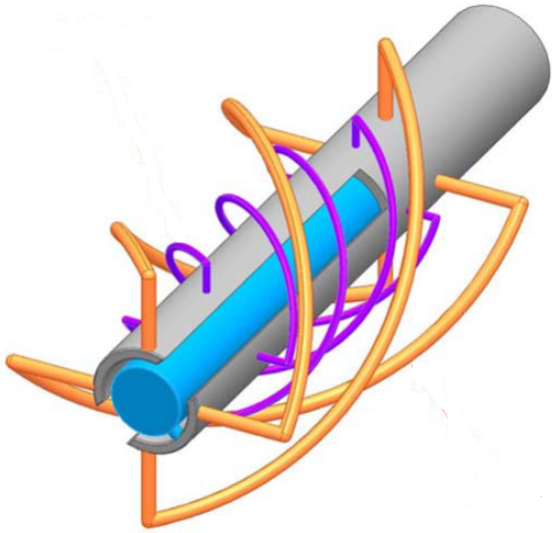

Figure 3.25: Dual band QHA using two single QHA's [Xudong Bai, 2014]

3.3 Truncated Spherical Helical Antenna

The Bifilar Truncated Spherical Helical Antenna (BTSHA) is a modification of the normal Spherical Helical Antenna (SHA) whos geometry is described by equation 3.10 to 3.12 where N is number of turns of the wire. The BTSHA is made upon two half's of the SHA which then is turned 180° to connect to each other. See figure 3.26.

$$r = a \tag{3.10}$$

$$\theta = cos^{-1}(\frac{\phi}{N\pi} - 1) \tag{3.11}$$

$$0 <= \phi <= 2\pi N \tag{3.12}$$

The BTSHA can be fed different ways using bottom feeding, side feeding or top feeding. One advantage using top feeding is that it can be fed using a "monopole" that will make a field inside the BTSHA together with the current flowing in opposite direction which makes it able to radiate in axial-null mode because of the symmetry. See figure 3.11. This makes it possible to archive better gain in the side direction as wanted for a satellite antenna for reception of ADS-B. Another advantage is the compact size compared to a conventional helical antenna. An important feature of this structure is that the angle of the cone can be adjusted by moving the height of the ground-plane. If the cone shall become broader the ground plane can be moved backward and if the cone is wanted narrower then the ground plane can be

formed as an reflector. Unfortunately the structure has a lack of gain in the center. Simulations has shown that the number of the wire turns has only little effect on the S-parameter and radiation pattern. A simulation has been made with the dimension $a = 2.86\lambda$, see figure 3.28. It is stated in [Clark, 2003] that the radiation pattern for this configuration should be omnidirectional. This has been shown not to be true and there is only two main-beams. The polarization is overall circular but with linear polarization in the direction of the two main-beams.

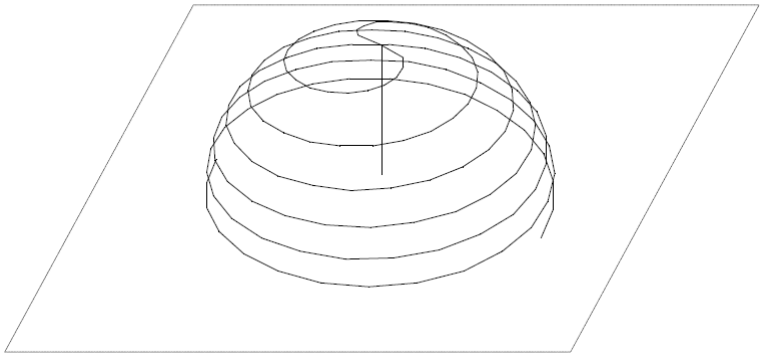

Figure 3.26: Bifilar Truncated Spherical Helical Antenna [Clark, 2003]

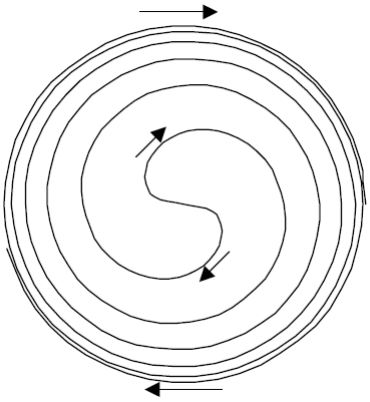

Figure 3.27: Currentflow of the BTSHA [Clark, 2003]

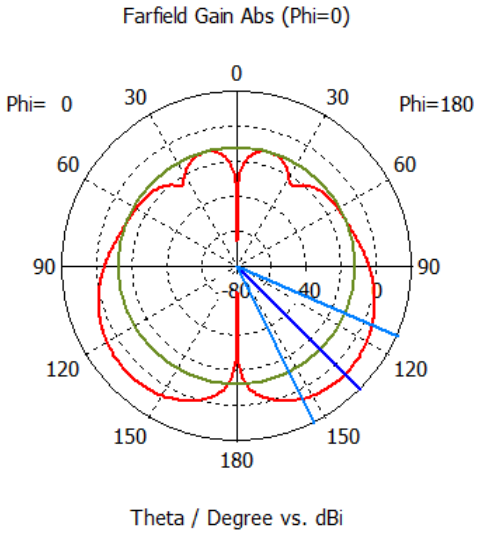

Figure 3.28: Farfield of a simulated BTSHA with $a = 2.86\lambda$ and $N = 1.5$. Maximal gain is 7.1dB. Be aware that the strucure at only this farfield is pointing at 180°

Another simulation has shown to have a more omnidirectional radiation pattern, which uses four arms instead of two (QTSHA) with a rotation of 90° each. Futher the structure is streched in the Z-direction by a factor of two. But still this structure has a lack of gain in the center. To overcome this problem simulations has shown that it is rather difficult to make a change to the structure that will increase the gain in the middle. The best solution to this problem is to change the feed point, see figure 3.31. The feeding point has been simulated for various points and a feeding point at 0.06λ from the top has shown to be the best. See figure 3.32. Unfortunately this asymmetry makes the polarization of the antenna more linear which then makes this option a bad decision.

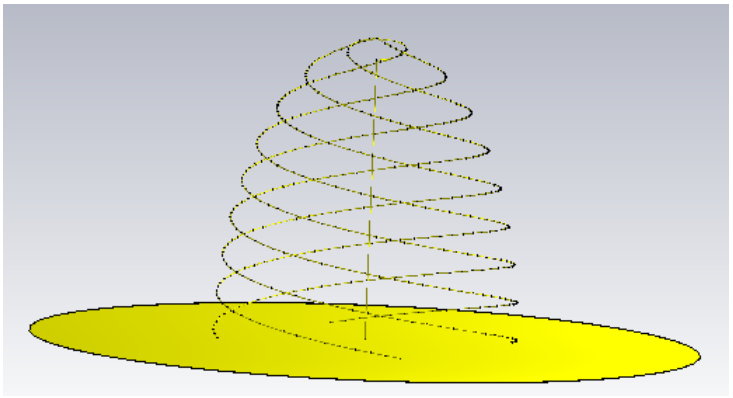

Figure 3.29: Stretched Quadrifilar Truncated Spherical Helical Antenna

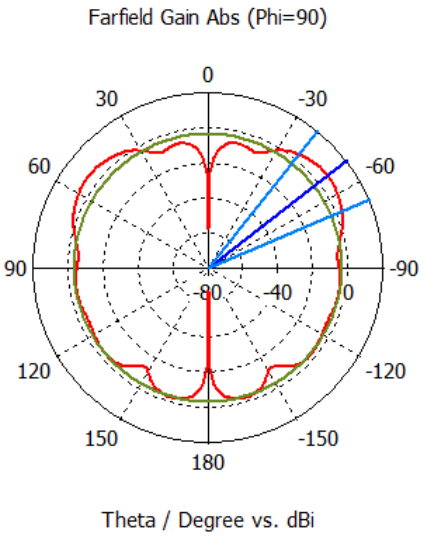

Figure 3.30: Farfield of a simulated QTSHA with $a = 2.86\lambda$ and $N = 1.5$. Maximal gain is 5.9dB

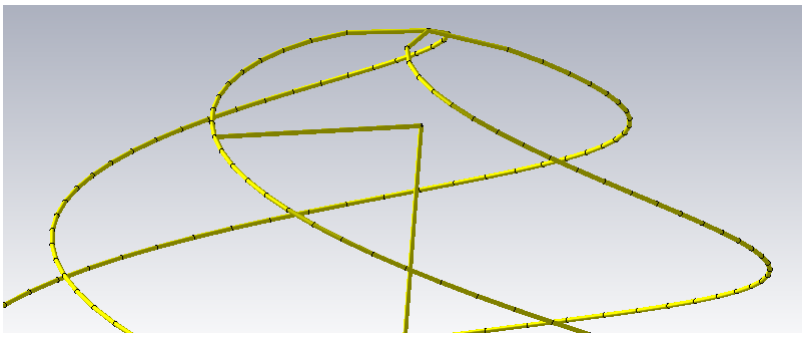

Figure 3.31: Position of the changed feeding point

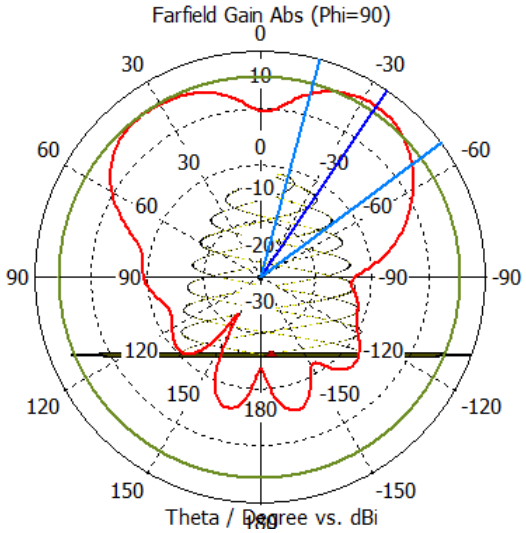

Figure 3.32: Farfield of a simulated QTSHA with $a = 2.86\lambda$ and $N = 1.5$. The figure is fully omnidirectional.

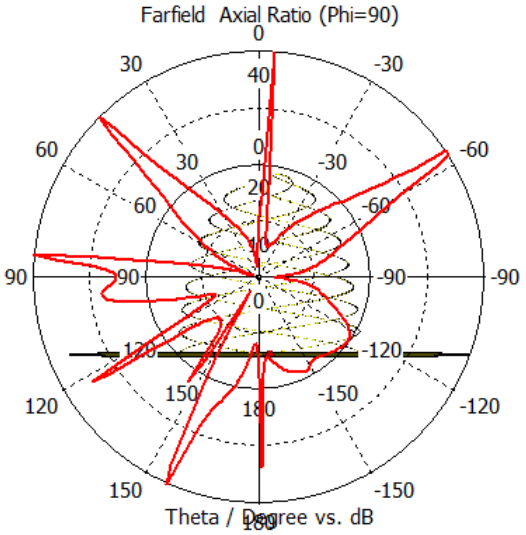

Figure 3.33: Axial ratio of the simulates antenna shows that this is not a circular polarized antenna

Chapter 4

Conclusion

In case you have questions, comments, suggestions or have found a bug, please do not hesitate to contact me. You can find my contact details below.

Jesper Kjær Nielsen
jkn@es.aau.dk
http://kom.aau.dk/~jkn
Niels Jernes Vej 12, A6-309
9220 Aalborg Ø

Bibliography

Balanis, C. A. (2005). *Antenna Theory Analysis And Design*. Wiley, 3. ed. edition.

Clark, J. R. (2003). Multifilar hemispherical helical antennas. Virginia Polytechnic Institute and State University.

Francis, e. a. (2011). The flying laboratory for the observation of ads-b signals. https://www.hindawi.com/journals/ijno/2011/973656/.

ITU-R (2017). Reception of automatic dependent surveillance broadcast via satellite and compatibility studies with incumbent systems in the frequency band 1087.7-1092.3 mhz. https://www.itu.int/dms_pub/itu-r/opb/rep/R-REP-M.2413-2017-PDF-E.pdf.

Iyer, V. (2010). Broadband impedance matching of antenna radiators. https://web.wpi.edu/Pubs/ETD/Available/etd-092910-012955/unrestricted/viyer.pdf.

Shkelzen Cakaj, e. a. (2014). The coverage analysis for low earth orbiting satellites at low elevation. International Journal of Advanced Computer Science and Applications, Vol. 5, No. 6, 2014.

Sun, J. (2015). The 1090mhz riddle. https://mode-s.org/decode/.

William A. Imbriale, e. a. (2012). *Space Antenna Handbook*. Wiley, 1. ed. edition.

Xiaoqiang Yang, e. a. (2014). A broadband printed quadrifilar helical antenna with a novel compact broadband feeding network. Progress In Electromagnetics Research C, Vol. 51, 103–109, 2014.

Xudong Bai, e. a. (2014). Compact design of triple-band circularly polarized quadrifilar helix antennas. IEEE antennas and wireless propagation letters, VOL. 13 2014.

Appendix A

Appendix A name

Here is the first appendix